NATIONAL ADVISORY COMMITTEE FOR AERONAUTICS

TECHNICAL MEMORANDUM

No. 1066

COMPARATIVE RESULTS OF TESTS ON SEVERAL DIFFERENT TYPES OF NOZZLES

By M. S. Kisenko

Central Aero-Hydrodynamical Institute

Washington
June 1944

NACA TM No. 1066

NATIONAL ADVISORY COMMITTEE FOR AERONAUTICS

TECHNICAL MEMORANDUM NO. 1066

COMPARATIVE RESULTS OF TESTS ON SEVERAL DIFFERENT TYPES OF NOZZLES*

By M. S. Kisenko

SUMMARY

This paper presents the results of tests conducted to determine the effect of the constructional elements of a Laval nozzle on the velocity and pressure distribution and the magnitude of the reaction force of the jet. The effect was studied of the shapes of the entrance section of the nozzle and three types of divergent sections: namely, straight cone, conoidal with cylindrical end piece and diffuser obtained computationally by a graphical method due to Professor F. I. Frankl. The effect of the divergence angle of the nozzle on the jet reaction was also investigated. The results of the investigation showed that the shape of the generator of the inner surface of the entrance part of the nozzle essentially has no effect on the character of the flow and on the reaction. The nozzle that was obtained by graphical computation assured the possibility of obtaining a flow for which the velocity of all the gas particles is parallel to the axis of symmetry of the nozzle, the reaction being on the average 2 to 3 percent greater than for the usual conical nozzle under the same conditions. For the conical nozzle the maximum reaction was obtained for a cone angle of 25° to 27°. At the end of this paper a sample computation is given by the graphical method. The tests were started at the beginning of 1936 and this paper was written at the same time.

INTRODUCTION

The operation of certain machines and apparatus, for example, steam or gas turbines, rocket motors, and wind

*Report No. 478 of the Central Aero-Hydrodynamical Institute, Moscow, 1940.

tunnels, is based on the transformation of the potential energy of the gas contained in a certain limited volume into kinetic energy of the jet flowing out of a container with a large velocity through nozzles of one type or another.

For obtaining jets with subsonic velocities cylindrical nozzles are used while conical nozzles (Laval nozzles) are used for supersonic velocities.

The theoretical velocity of outflow is generally denoted as that velocity w' which would be obtained if the flow process were a reversible adiabatic or isentropic process, that is, if the condition were satisfied

$$ds = 0$$

or

$$Tds = d\theta - \frac{dp}{\rho} = 0$$

where

T absolute temperature of the gas

θ heat content or enthalpy

s entropy

p pressure

ρ density

Actually the flow process is not reversible and isentropic. The transfer of heat to the nozzle walls and the friction of the gas particles at the walls lead to an increase in the entropy so that always $ds > 0$. The true velocity w will, therefore, be less than the theoretical velocity w'. The ratio of these two velocities is denoted as the velocity coefficient $\varphi = w/w'$.

It should be noted that the transformation in the nozzle of the potential energy into kinetic occurs with a high degree of efficiency. The velocity coefficient φ even for a nozzle with rough inner surface is still

near unity and does not drop below 0.92. For nozzles with a highly polished surface and of a correctly designed shape φ reaches a value of the order of 0.98.

Another important criterion for judging the quality of a nozzle is the ratio of the true discharge G in unit time to the theoretical discharge G'. This ratio is denoted as the discharge coefficient through the nozzle: $\mu = G/G'$.

The coefficients φ and μ depend on the initial state of the gas, the degree of expansion of the gas in the nozzle, and apparently, on the geometric characteristics of the latter. The values of φ and μ for each nozzle are determined experimentally. In particular, the coefficient φ may be computed as the ratio of the momentums obtained experimentally to the theoretical (assuming $\mu = 1$). (This assumption is admissible only for comparison purposes. In general, however, μ is always less than unity.) Thus, knowing the discharge rate per second G, and the force of reaction obtained experimentally, and remembering that

$$P = \frac{Gw}{g} = mw,$$

while the theoretical reaction of the jet is

$$P' = \frac{Gw'}{g} = mw'$$

there is obtained

$$\varphi = \frac{P}{P'} \qquad (1)$$

A correctly chosen shape of nozzle should assure a flow with uniformly distributed velocities and static pressures both in the transverse and longitudinal sections of the flow. The direction of the velocity of all the particles of gas should be parallel to the axis of symmetry of the nozzle.

In the case of nozzles for turbines and rockets the satisfaction of these requirements is necessary in order to avoid losses in momentum. For nozzles of wind tunnels,

however, the condition of parallel velocities of the gas particles must be satisfied since otherwise the character of the flow about the bodies tested in the tunnels would not be similar to the flow in free flight.

In this paper the results are presented of tests undertaken with the special purpose of determining the effect of the constructional elements of the nozzle on the magnitude of the reaction of the jet and on the character of the velocity and pressure distribution in the flow.

TEST PROCEDURE

The reaction of the jet can be measured by two methods. By one method the impulse of the jet is measured with the aid of a disk mounted normal to the direction of the jet and connected with a dynamometer (fig. 1). Knowing the rate of discharge per second the true velocity of the flow can be determined by the momentum equation.

Thus, if P is the thrust measured by the dynamometer, m the mass of air flowing per second assumed constant, and w the flow velocity then by definition:

$$P = mw \tag{2}$$

whence

$$w = \frac{P}{m} \tag{3}$$

The other method is based on the direct measurement of the jet reaction expressed by equation (2). In general, equation (2) is valid only in the case that p_a – the pressure of the gas in the outlet cross-section of the nozzle – and p_o – the pressure of the external medium – are strictly equal to each other. The nozzle satisfying the condition $p_a = p_o$ will be denoted as the normal or computed nozzle. In the case of the inequality $p_a \neq p_o$ equation (2) must be replaced by the expression

$$P = mw + f_a(p_a - p_o) \tag{4}$$

where f_a is the area of the outlet section of the nozzle. The last term on the right side of the above equation is the static term.

Actually a nozzle rarely operates under the computational assumed conditions and therefore the investigation of the effect of the static term on the value of the thrust is of considerable practical interest. In order to measure the reaction of the jet by the second method an apparatus was constructed (general view shown on figs. 2 and 3). The tube 1 serves to conduct the compressed air to cylinder 2 which, with the aid of a flange, is connected to tube 1. Cylinder 2 is surrounded on top by a jacket 3 which at its upper end is supported against the ball bearing 6 and can rotate about cylinder 2. To cylinder 3 on the two diametrically opposite sides are attached two tubes 5 and 5a. To tube 5 is attached the weight 9 as a counterweight of chamber 7 with the tested nozzle 8 attached to tube 5a. A long thin manometer tube is attached to connecting tube 11. In the case where the working gas consists of the products of combustion the spark plugs 14 serve to ignite the fuel mixture. For the same purpose an opening is provided for mounting a spark plug in chamber 7. To make cylinder 3 airtight a labyrinth packing is placed between the outer surface of the cylinder and the inner surface of the jacket 3. Moreover, for the same purpose the water between cylinders 2 and 3 was put under a certain pressure, greater than the pressure in cylinder 2. The water is supplied through tube 13. In working with the products of combustion this water serves also to cool cylinder 2. Practical operation of the apparatus showed that the hermetic sealing of cylinder 2 was assured by the labyrinth packing alone and there was no need of a water back pressure. The fiber plate 10 serves as a safety valve in case of a sudden rise in pressure in cylinder 2. Chamber 7 is supported at the bottom on the dynamometer with the aid of which the reaction force is measured. The apparatus also permits the carrying out of a qualitative comparison of two nozzles. For this purpose, in place of the plug 12 in chamber 7, a second nozzle is screwed in the reaction of which is directed opposite to that of nozzle 8.

To measure the rate of discharge of the air through the nozzle a so-called diaphragm is placed in pipe 1 (not shown on the sketch). The pressure difference h at the inlet and outlet of the diaphram is measured by a differential manometer of the Yasinsky type. The first term in expression (4) for the reaction force of the jet, that is, the momentum, is measured near the nozzle by a dynamometer with disk placed normal to the nozzle axis, the distance from the outlet section of the nozzle to the center of the disk should not be greater than two diameters of the jet in order to avoid the unfavorable distorting action of the disturbed outside air sucked in by the jet.

The dynamic head was measured with the aid of a system of Pitot tubes mounted on the disk for measuring the momentum (fig. 4), the distance between the individual tubes being equal to 5 millimeters. By displacing the tubes along the axis of the jet the true dynamic pressures along the diameter and along the axis of the jet may be determined.

Knowing the value of the dynamic pressure for a given point it is not difficult by the known formula of Raleigh (reference 1) to obtain the true velocity. From numerous tests it was found that the values of the velocities obtained by this formula are very nearly the true flow velocities.

Figure 5 gives the curve, computed by the Raleigh formula, of the dynamic pressure in a supersonic jet flow as a function of the Bairstow (or Mach) number (w/c). This curve may be used to determine the actual velocity of the supersonic flow (or the value of w/c) from the dynamic pressure experimentally obtained.

The temperature in the chamber ahead of the diverging nozzle was measured with a thermocouple. The temperature of the air in the flow was determined on the assumption of adiabatic expansion of the gas in the nozzle by the formula:

$$T = T_i \left(\frac{p}{p_i}\right)^{\frac{k-1}{k}} \qquad (7)$$

where

T_i and p_i temperature and pressure of the gas in the chamber

T and P corresponding parameters after expansion

k ratio of specific heats

The static pressure in the flow was measured by a tube placed in the gas flow with its axis parallel to the velocity direction. Figure 6 shows the static tube mounted in the flow.

Besides determining the above thermodynamic parameters the flow spectrum was also photographed by the Tepler method during the tests.

GAS JET OF SUPERSONIC VELOCITY

In investigating the motion of gases with small velocity the phenomenon of compressibility is generally not taken into account. The error in the pressure computations of the flow with the compressibility neglected constitutes about 2 percent at speeds of 100 meters per second. At speeds of the order of 200 meters per second, however, this error is more appreciable and constitutes about 9 percent while for $w = 340$ meters per second, that is, for flow velocities equal to the velocity of sound, the error reaches 27.5 percent.

Figure 7 shows the law of velocity distribution in the transverse cross-section and figure 8 the velocity and static pressure distribution along the flow axis for a conical Laval nozzle. As may be seen from the curves the velocities and static pressures in both in the transverse and axial sections are not constant. The sharp, almost periodical fluctuations in the values of the static pressures are explained by the fact that in the sonic and supersonic flow a very complicated system of stationary waves arises. These waves were first observed by Ernst Mach in whose honor they are called Mach waves.

To explain the physical nature of the Mach waves a two-dimensional flow with velocity greater than that of sound is considered (fig. 9). It is assumed that the pressure in the outlet cross section of the nozzle p_a is greater than the pressure p_o of the external medium. At the outlet section at point A a disturbance then arises as a result of the discontinuous pressure drop from p_a to p_o. The rarefaction wave having a velocity always equal to the local velocity of sound is propagated only as far as the line AB. The latter is a Mach wave and is essentially the envelope of all the sound waves arising at point A. The Mach wave AB is thus the boundary of the rarefaction disturbance starting at point A. The expansion of the gas in the region ABC from p_a to p_o produces a change in the radial velocities of the flow particles as a result of which the direction of the flow from line AB deviates toward the outside until the pressure is equal to that of the outside medium (line AC) after which the flow again becomes straight. In the case where the pressure in the outlet section of the nozzle is less than the pressure

of the outside medium, that is, $p_a < p_o$, the deviation of the flow will be directed inward. Therefore in the first case, that is, $p_a > p_o$ the diameter of the flow will be greater than the diameter of the outlet section of the nozzle while in the second case, $p_a < p_o$ the diameter of the flow will be less than that of the outlet section. In this case the line AC is absent from the flow spectrum. Thus in a flow with axial symmetry the expansion due to the inequality of p_a and p_o will occur in the region included between the two conical Mach surfaces with the corresponding generators AB and AC. In the region lying ahead of the Mach line AB the disturbing effect of point A is entirely absent and the pressure in this part of the flow remains equal to the pressure in the nozzle cross-section.

The angle of inclination of the Mach wave α is determined by the ratio of the local velocity of sound to the velocity of the gas before expansion and the angle α' by the same ratio after expansion, that is,

$$\sin \alpha = \frac{c}{w} \tag{8}$$

The Mach wave diagrams of the supersonic plane-parallel flow for $p_a > p_o$ and $p_a < p_o$ are shown in figure 10 and 11. The spectrum of the flow for $p_a > p_o$ is considered. The rarefaction wave AC on reaching the boundary layer of the jet is reflected toward the inside of the jet in the form of compression waves (the compression waves are drawn full line and the rarefaction waves dotted). In regions 2, 3, 5, and 6 the static pressure is equal to the pressure of the surrounding medium, while in region 4, separated from the outlet section of the nozzle by a distance of two rarefaction waves, the prevailing pressure will be lower. In region 7, immediately behind the compression waves, the pressure will be the same as in region 1, and there is, therefore, a definite disturbance period present. Analogous considerations apply to the relations of figure 11. The waves AC and A_1C_1 in this case will be compression waves and there will be corresponding regions of increased and lowered pressures.

The above description of plane-parallel flow cannot without reservations be entirely identified with the flow

with axial symmetry because the actual flow is three dimensional and a Mach wave will be formed at each point on the circumference of the outlet section.

The Mach waves may be formed not only in the flow behind the outlet section of the nozzle but also within the nozzle. The latter waves will occur only in case the nozzle has a large divergence angle, as a result of which the flow separates from the walls even within the nozzles, or in case of a very rough inner nozzle surface.

On the basis of what has already been said the conclusion may be drawn that the nonuniformity of the static pressure distribution in the supersonic flow is explained by the presence of Mach waves in the flow. This conclusion is entirely confirmed also by the results of the tests conducted. Besides the effect of the stationary sound waves the friction of the gas particles at the nozzle walls and at the external medium also affects the transverse and axial velocity distribution.

There is still another factor that must be mentioned which affects the velocity distribution of the flow. As test results have shown, the diameter of the flow, with increasing distance from the outlet section of the nozzle increases as a result of the sucking in of the outer air by the jet. This suction takes place with simultaneous decrease in velocity along the jet. To investigate this phenomenon the following tests were conducted. A screen of thin constantan wires stretched on two porcelain rods was mounted near the jet escaping from the Laval nozzle. The wires were heated to a red heat by an electric current passed through them. The Teplor photograph (fig. 12) shows clearly the direction of motion of those air particles which before being sucked into the stream passed by the heated wires. As may be seen from the photograph the suction begins at the outlet section of the nozzle. Evidently, with increasing distance from the nozzle the quantity of air sucked into the air stream increases and therefore the flow velocity correspondingly decreases, the decrease being greatest at the boundary layer.

It should also be mentioned that the flow obtained for nozzles with $p_a \neq p_o$ will always have nonuniform velocity and pressure distributions as a result of vortex formation and the dissipation of the jet at the outlet section of the nozzle.

EFFECT OF STRUCTURAL ELEMENTS OF THE NOZZLE ON THE THRUST AND CHARACATER OF THE FLOW

The nozzle cavity (fig. 13) is divided into two parts. The first part converges toward the narrowest critical section while the second part is a diverging cone having an 8° to 12° cone angle. The effect of each of these parts on the character of the flow and on the magnitude of the reaction force of the jet with the object of finding the most rational shape of nozzle is to be considered.

Converging Part of Nozzle

In this case if the flow into the nozzle is from a vessel whose volume is many times greater than the volume discharged per second the velocity of the gas at the convergent section is generally neglected so that the shape of the first part is likewise not taken into account. The only requirement for this part of the nozzle is that it should be carefully rounded and that it should assure a smooth flow of the gases. The smoothing curve is chosen on an intuitive basis. Considering, however, the motion of the gas in this part of the nozzle as analogous to the motion of a fluid in a curved channel it may be concluded that as a result of the curvature of the path centrifugal pressures occur in the flow. The direction of these pressures will always be away from the center of curvature. Hence in the first part of the nozzle the pressure near the axis will be greater than at the walls. Near the critical section the opposite will be true since at this place the curvature of the walls is reversed with the center of curvature outside the nozzle cavity. It is thus clear that the pressure and velocity distributions in this part of the nozzle will depend on the radii of curvature of the inner surface of the nozzle. From investigations of the nozzles of wind tunnels of supersonic velocities in various aerodynamic laboratories the dependence of the character of the flow on the shape of the generator of the inner surface at the entrance part of the nozzle was established. The nozzles of wind tunnels of subsonic velocities have no second (divergent) part.

Figure 14 shows the distribution of the dynamic pressures q in the flow cross-section for two nozzles with

different shapes of entrance parts and figure 15 shows the distribution of the dynamic pressures q and static pressures λ along the axis for the same nozzles (reference 2). The dotted curves were obtained for nozzles for which the generator of the entrance part is a lemniscate and at the outlet is an arc of a circle (CAHI T-5). The continuous curves were obtained for nozzles whose inner contours were constructed by the formula

$$r = \frac{r_0}{\sqrt{1 - \left[1 - \left(\frac{r_0}{r_1}\right)^2\right] \frac{\left(1 - \frac{3z^2}{a^2}\right)^2}{\left(1 + \frac{z^2}{a^2}\right)^3}}} \qquad (9)$$

where

r_0 radius of the outlet section

r_1 radius of the inlet section

r variable radius at the distance z from the origin of coordinates

$a/\sqrt{3}$ length of the projection of the curve on the z-axis

From the tests conducted at CAHI it was found that it was best to take

$$\frac{a}{\sqrt{3}} = 4.14\ r_0$$

This formula was obtained by Witoszynski (reference 3) and represents the case of a particular solution of the Laplace equation for the stream function (reference 3). As may be seen from figures 14 and 15 the velocity and static pressure distributions in the flow are more satisfactory for the nozzle computed by Witoszynski.

With the object of determining the effect on the reaction force of the shape of the first part of a nozzle having also a diverging part (Laval nozzle) the following tests were conducted. Three nozzles were prepared: 1, 2, and 3 (fig. 16), for which the diverging parts were entirely the same, that is, the diameter of the outlet section d_a,

the diameter of the critical section d_c and the cone angle α were equal but the shapes of the entrance parts were different. The shape of the curve for the entrance part of nozzle 1 was constructed according to the Witoszynski equation. Nozzle 2 differed from nozzle 1 in that the former had two rings at the entrance part. Finally, nozzle 3 had a nonstreamline shape for the entrance part. All three nozzles were computed for $w/c = 2.64$. The thrusts of the nozzles were measured by the reaction method on the apparatus previously described. In table 1 the values of the measured thrust and the velocity coefficients φ computed by formula (1) are given.

TABLE 1

Nozzle	P kg	φ	Percent
1	30.3	0.965	100
2	29.9	.953	98.7
3	29.8	.950	98.2

The magnitude of the theoretical impulse P' was determined on the basis of the following considerations. The thermodynamic parameters of the air in the chamber during the test were taken as the following: $p_i = 21.5$ atmospheres, $T_i = 273^\circ$. Remembering that the flow is open the static pressure in the flow may be taken approximately equal to the pressure of the external medium, that is, $p = 1$ atmosphere. The temperature of the air in the flow was computed by formula (7)

$$T = T_i \left(\frac{p}{p_i}\right)^{\frac{k-1}{k}}$$

The theoretical absolute velocity of the flow was found from the equation

$$w' = \sqrt{2g \frac{k}{k-1} RT \left[1 - \left(\frac{p}{p_i}\right)^{\frac{k-1}{k}}\right]} \qquad (10)$$

and the theoretical discharge per second through the nozzle obtained from the expression

$$G = \frac{w'f_a}{v} \qquad (11)$$

where v is the specific volume of gas in the flow. Substituting the numerical values there is obtained

$T = 115^{\circ}$, $w' = 565$ meters per second, $G = 0.545$ kilogram per second. Hence the theoretical thrust of the nozzle is equal to

$$P' = mw' = \frac{0.545}{9.81} 565 = 31.4 \text{ kilograms}$$

The maximum thrust obtained from the tests on nozzle 1 was equal to 30.3 kilograms. As may be seen from table 1 the values of the velocity coefficients obtained for all three nozzles do not exceed the limits of the values usually assumed in the computations. For nozzle 3, having an entrance part of unfavorable shape the velocity coefficient φ is 1.8 percent less than the value 100 assumed for nozzle 1; for nozzle 2 φ was only 1.3 percent less.

It must be said that the effect of an improvement in shape of the first part of the nozzle on the coefficient φ is negligible and lies within the limits of experimental error. Remembering, however, that the values of φ were obtained as the average values of a large number of tests (not less than 15 tests for each nozzle) these values may be considered as entirely satisfactory.

The flow spectra obtained by the Tepler method are similar for all three nozzles. Evidently a change in shape of the first part of a Laval nozzle has no effect on the velocity and static pressure distributions in the flow.

Divergent Part of the Nozzle

Depending on the ratio of dimensions of the outlet and critical cross-sections in the conical part the expansion of the gases is accompanied by a drop in pressure from

that at the critical section $p_c = 0.528\ p_i$ (for air) to the outside pressure. In the case of nozzles for which the ratio of the cone diameters was assumed greater than the design value the pressure inside the cone may drop below the pressure of the external medium (back pressure). As a result of this expansion the pressure rise at the outlet occurs abruptly being accompanied by a loss in velocity.

The character of the velocity and static pressure distribution in the flow from a conical nozzle depends chiefly on the structural elements of the second part, that is, on the ratio d_a/d_c or, for a given length of nozzle on the divergence angle α and also on the contour of the inner surface of the nozzle.

Possession of a general solution of the problem of the optimum shape of the divergent part of the nozzle is not yet obtained. Some investigators, it is true, have succeeded in solving this problem, experimentally, for certain conditions. Stanton found empirically the shape of the nozzle for the supersonic velocity wind tunnel at the National Physical Laboratory. This nozzle gives a flow free from Mach waves in the working part of the tunnel. The Stanton nozzle differed from the usual Laval nozzle in that the divergence angle of the conical part did not exceed 5° as compared with 10° to 12° usually assumed for the Laval nozzle. In addition the conical part of the nozzle smoothly passes over into a cylindrical piece at the outlet.

Figure 17 shows the curves of variation of the static pressure p and velocity w for this nozzle. As may be seen from the curves the cylindrical part has an interval where the curves p and w are almost parallel to the nozzle axis, that is, constant. This part was the one chosen for the test model. The dotted curves on the figure give the nozzle shape computed under conditions of adiabatic expansion of the air in the nozzle without taking account of the decrease in velocity due to friction at the wall. This confirms the adiabatic law of expansion of the air in the nozzle.

With the object of studying the effect on the character of the flow of the shape of the curve generating the second part of the nozzle a number of nozzles with conoidal inner surface and cylindrical piece at the outlet were investigated. The nozzles were tested for $w/c = 1.41$, 1.82, 2.24, and 2.74.

The results of all the tests were similar and therefore the test results for only one nozzle for $v/c = 1.82$ are given. The static pressures measured along the flow axis at various heights (H mm) from the outlet section are given for this nozzle in table 2. The temperature of the air in the flow behind the nozzle was computed by formula (7) on the basis of the measured air temperature in the chamber.

TABLE 2

Test	H (mm)	t_1 °C	t° C	p (atm)	Test	H (mm)	t_1 °D	t° C	p (atm)
1	5	190	8	0.742	11	50	0	-110	1.20
2	15	195	9	.749	12	60	0	-110	1.40
3	25	185	3	1.10	13	60	0	-110	1.40
4	30	200	13	.667	14	60	0	-110	1.40
5	30	185	3	.680	15	70	0	-110	1.25
6	40	195	9	1.10	16	70	0	-110	1.25
7	40	0	110	1.20	17	80	0	-110	.910
8	40	0	-110	1.20	18	80	0	-110	.922
9	50	0	-110	1.20	19	90	0	-110	.624
10	50	0	-110	1.20	20	90	0	-110	.624

From the data of table 2 the curve of static pressure distribution along the flow axis was drawn (fig. 18). As may be seen from the curve the static pressure distribution is extremely variable. The pressure gradient at the center of the jet reaches a value of the order of ±0.4 atmosphere. In order to eliminate the effect of possible accidental errors the measurements for a few points were repeated on various days. The scatter of the test points obtained in certain cases may apparently be explained by the effect of the variable atmospheric conditions (temperature and barometric pressure) not taken into account.

Comparing this curve with that of the static pressure curve at the center of the flow obtained by Stanton for the usual conical nozzle (fig. 8) the agreement of the law of variation of static pressures along the axis of the flow can be readily established. The curve given here is reversed (mirror reflection) with respect to the Stanton curve, a fact which is evidently explained by the different procedure in evaluating the test results. Figure 18 also

shows the curve of velocity distribution (w/c) measured along the flow axis. As may be seen from the curve the velocity at the center of the jet over a distance from 50 to 90 millimeters from the outlet section is almost constant. For the conical nozzle (fig. 8) the curve w/c cannot be assumed constant over any part of the flow.

Tests were also conducted for measuring the static pressure p_r at various distances r from the flow axis. The results of these tests are given in table 3.

TABLE 3

H (mm)	r (mm)	p_r (atm)	p (atm) (center)
40	10	1.00	1.20
40	6	1.00	
60	7	1.26	1.40
60	10	1.20	
70	10	1.20	1.25

The pressures at the center of the jet are greater than the pressures at the periphery.

The cross-sectional velocity distribution for the same nozzle, as may be seen from the experimental test curves (fig. 19), is more satisfactory than for the conical Laval nozzle (fig. 7). On this basis it may be concluded that the conoidal shape with cylindrical end piece gives a considerably better (cross-sectional and axial) velocity distribution than the Laval nozzle. The nonuniformity of the static pressure is, however, also maintained for the conoidal nozzle.

In 1934 Frankl (reference 4) published a method of graphical construction of the second part of the nozzle. This method is based on the theory of characteristics and

is an application of the method of Prandtl and Busemann, developed by them for plane-parallel flow, to the case of flow with axial symmetry.

Figure 20 shows a nozzle constructed graphically by the Frankl method. The dotted lines indicate the contours of the usual conical nozzle with the same ratio d_a/d_c as for the Frankl nozzle.

Figure 21 shows the curves of the static pressure gradient along the flow axis for the Frankl nozzle for $w/c = 1.47$. The pressure gradient for the design condition ($p_i = 3.49$ atm) does not exceed ± 0.02 atm.. For the case where the nozzle operates at other than design conditions ($p_i = 4$ atm) the axial static pressure distribution is less satisfactory as compared with the design conditions. The same figure gives the curve of velocity variation along the flow axis. As may be seen from the curve the velocity remains constant at a distance of 30 to 90 millimeters from the outlet section.

For the same nozzle tests were conducted on the transverse velocity distribution. The results are given on figure 22. For the design conditions (full curves) the velocities over the cross-section are uniform with a slight drop at the boundary of the flow. Near the exit section of the nozzle the nonuniformity of the velocities is greater. The dotted curves show the velocity distribution for pressures of 4, 5, and 6 atmospheres. As may be seen from the curves, the Frankl nozzle for other than design conditions gives a flow with nonuniform cross-sectional velocity distribution.

For the same nozzle the reaction of the jet was measured. It was found that the thrust for the nozzle computed according to Frankl is approximately 2.5 to 3 percent greater than the thrust of the usual conical nozzle with same d_a/d_c ratio. In the case of application of this nozzle to rocket apparatus, however, it is necessary to take account of the fact that the length of the Frankl nozzle is almost twice its equivalent conical nozzle. Therefore the heat losses over the nozzle surface during prolonged operation of the rocket motor will be greater than for the conical nozzle.

Simultaneously with the tests for $w/c = 1.47$ tests were also conducted for the Frankl nozzle for $w/c = 1.47$, 1.62, 1.76, 2.06, and 2.64. The curves of dynamic and static pressure distributions obtained for these nozzles are similar

to the curves for the nozzle for $w/c = 1.47$. The pressure gradient along the flow axis for $w/c = 2.64$ is given in table 4.

TABLE 4

H (mm)	0	20	40	60	80	100
P (atm)	0.95	0.90	1.00	0.99	0.90	1.02

The cross-sectional velocity distribution for the same nozzle is shown on figure 23. Unfortunately, the investigation of the nozzle flow for $w/c = 2.64$ was carried out at the sections near the outlet of the nozzle (20, 30, and 40 mm) and, as previously stated, in this region of flow, for the nozzles computed by the Frankl method, a certain nonuniformity is observed in the velocity distribution. As the distance from the outlet edge increases, however, the character of the velocity distribution improves.

The lack of uniformity of the velocities at the outlet section of the nozzle may be explained by the fact that the back pressure at the outlet is not exactly equal to the computation value due to the variation of the barometric pressure. For this reason near the outlet section disturbances appear which affect the character of the flow. In order to assure the rated operating conditions of the Frankl nozzle it is necessary each time to choose the magnitude p_i as a function of the atmospheric pressure maintaining the design ratio p_o/p_i.

As may be seen from the curves of figure 23, on approaching the boundaries, the velocities are not lowered for the part of the flow investigated and the test points lie on one line. This is evidently explained by the fact that at large velocities in the flow region near the nozzle outlet section no mixing of the gas of the boundary layer with the outside air occurs. The boundary layer particles having a large forward velocity form as it were a firm wall relative to the outside medium and the flow occurs with small friction in the tube formed by the surrounding air.

In passing from the computation pressure in the chamber $p_i = 21.5$ atmospheres to 22 atmospheres the uniformity of

the velocities is maintained with a slight increase in the velocity in absolute value.

Figures 24 and 25 show the flow spectra obtained for $w/c = 2.64$ with the conical Laval nozzle and with the nozzle computed by Frankl. Both nozzles have the same ratio d_a/d_c and the same pressure in the chamber $p = 21.5$ atmospheres. In order to maintain the same external conditions (atm pressure and air temp.) both photographs were taken on the same day. As may be seen from the photographs, instead of the complicated system of stationary waves formed in the flow of the conical nozzle only weak Mach waves are observed in the Frankl nozzle. Moreover the flow in a latter remains cylindrical over a considerable distance from the nozzle. In the ideal case, that is, for strict maintenance of the ratio p_o/p_i and careful polishing of the walls the Frankl nozzle should not give any Mach waves in the flow at all.

It has already been shown that to satisfy accurately these conditions is almost impossible due to the fluctuations of the atmospherical conditions. Hence the Mach waves in a supersonic flow are unavoidable; but their intensity, as may be seen on figure 25, is very small in the Frankl nozzle.

In conclusion it may be said that of the three possible shapes considered of the second part of the nozzle; namely, (1) the conical, (2) conoidal with cylindrical piece, and (3) nozzle computed by Frankl, the latter best satisfies the requirements imposed on the nozzle. An example of a nozzle computation by the Frankl method is given.

Effect of the Divergence Angle

From what has previously been said it is clear that the cone angle of the second part of the nozzle may be either constant along the nozzle axis or variable. The most favorable nozzle from the point of view of the heat losses should have the maximum possible divergence since the length and surface area will then be the least.

With the object of investigating the effect of the cone angle on the reaction a number of nozzles with constant ratio $d_a/d_c = 1.73$ were tested, the cone angle being varied from 10° to 30°. The pressure and temperature of the

air in the chamber for all tests were constant and equal: $p_i = 21.5$ atmospheres, $T_i = 273^\circ$ absolute.

Figure 26 shows the dependence of the nozzle thrust on the cone angle for rated and nonrated operating conditions. For the assumed initial thermodynamic parameters of the air and for the design conditions the most favorable value of the cone angle evidently lies near 25°, since with further increase in the angle the thrust curve remains almost parallel to the axis of abscissas. It may be stated that the magnitude of the reaction depends very little on the divergence of the nozzle. This conclusion agrees with the results of the tests conducted under different conditions, in particular for nonstationary flows. To arrive at more definite conclusions it would be necessary to conduct tests on nozzles with cone angle greater than 30° in order to determine the point of inflection of the curve of reaction force.

In addition to the tests described above, measurements were made on the reaction of the jet for a nozzle with cone angle $\alpha = 12^\circ$ for various values of d_a/d_c, obtained by simply shortening the same nozzle. The results are given on figure 27. The theoretical values of the thrust P_{th} are computed by formula (4). The maximum test value of the thrust was obtained for the design ratio $d_a/d_c = 1.73$ and was equal to 18.8 kilograms. For $d_a/d_c = 1$, that is, in the absence of any divergence the thrust was equal to 17 kilograms, that is, only 11.0 percent less than for the design nozzle. Therefore in working with a cold gas, when no heating occurs, the part played by the divergence of the nozzle in producing the thrust is relatively small.

These tests also made it possible to determine the character of the changes in the two terms entering the expression for the nozzle thrust (equation 4). The results are given in figure 28 from which it is seen that with increasing value of p_a the value of the component nw rapidly drops. On table 5 the relative values of both components for certain values of p_a are given.

TABLE 5

p_a (atm)	1	1.6	2.8	5.4	11.2
P (kg)	22.7	22.5	22.2	21.0	20.1
mw:P	1	0.95	0.89	0.80	0.605
$f_a(p_a - p_o)$:P	0	0.05	0.11	0.20	0.395

As may be seen from the table the value of the static term increases with increasing p_a and for $p_a = 11.2$ atmospheres constitutes 39.5 percent of the total thrust of the nozzle. For the usual conditions, however, when the lowering of the back pressure, due to inaccurate computation of the nozzle or to a change in the atmospheric conditions, does not exceed 0.5 to 0.6 atmospheres the magnitude of the static term does not exceed 5 percent of the total thrust of the nozzle. The total nozzle thrust slowly decreases with increasing p_a due to the losses in the discontinuous pressure change at the nozzle outlet.

CONCLUSIONS

The results of the conducted tests provide a basis for certain conclusions which should be taken into account in selecting the shape of the nozzle:

(1) The shape of the entrance part of the nozzle does not show any large effect on the character of the flow and therefore the choice of any particular shape is conditioned chiefly by the structural considerations.

(2) The nozzle with exit part conoidal and ending with a cylindrical piece gives a better velocity distribution in the transverse and longitudinal sections of the flow than the Laval nozzle but with regard to the static pressure distribution it does not differ from the usual conical nozzle.

(3) The nozzle computed by the Frankl method gives a parallel flow with uniformly distributed velocities and static pressures both in the transverse and longitudinal sections. The reaction of the jet obtained with this nozzle

is on the average 2 to 3 percent greater than in the usual nozzle under the same conditions.

(4) The maximum reaction is obtained for a cone angle of 20° to 25° and for the normal value of d_a/d_c, that is, under the condition that the pressure at the outlet section of the nozzle is equal to the pressure in the surrounding medium. In the absence of the second part of the nozzle the reaction is found to be 11.0 percent less than for the computed nozzle.

EXAMPLE OF NOZZLE COMPUTATION BY THE FRANKL METHOD

The theoretical basis of the graphical method of constructing a nozzle of axial symmetry together with a short discussion of its practical applications is given in the Frankl article (reference 4). In order to make this method available not only to engineers but also to less qualified workers a detailed numerical computation of a nozzle for a velocity $w = 900$ meters per second is given.

The nozzle (fig. 29) is divided into four parts:

(1) The part of the nozzle in which the air is conducted to the critical section.

(2) The critical section (throat)

(3) The part between the critical section and the streamline part of the nozzle, the generator of the surface of this part being a straight line (cone)

(4) Streamline part of the nozzle whose generating curve is obtained by the graphical method

The shape of the curve of the first part of the nozzle is not computed but is chosen arbitrarily on the basis of considerations of smooth conduction of the air to the critical section. To compute the critical section it is necessary to have data on the initial condition of the air in the chamber (before expansion in the nozzle) and know the rate of discharge per second through the nozzle. These data are generally obtained by a preliminary computation. The initial parameters for computing the nozzle are denoted by the following symbols:

G rate of discharge of the products of combustion, kg/sec

f_i initial area of the entrance part, m^2

p_i initial pressure (pressure in the chamber), kg/cm^2

v_i initial specific volume of air, m^3/kg

T_i initial absolute temperature of the air

w_i initial velocity, m/sec

With these values given the area of the critical section f_c and all the thermodynamic parameters associated with it are obtained:

$$T_c, w_c, \text{ and } v_c$$

Since in rocket motors and in wind tunnels of large velocity it is desirable to have velocities much greater than the velocity of sound

$$\frac{p_o}{p_i} > \beta \quad \text{where} \quad \beta = \left(\frac{2}{k-1}\right)^{\frac{k}{k-1}}$$

With this in mind use is made of the corresponding formulas of the flow of gases, given in any book on thermodynamics. The process of expansion of the gas in the nozzle is assumed to be adiabatic. From the formula

$$\frac{G}{f_c} = \left(\frac{2}{k+1}\right)^{\frac{1}{k-1}} \sqrt{\frac{2gk}{k+1}} \sqrt{\frac{p_i}{v_i}} \qquad (1)$$

the area of the critical section of the nozzle may be determined. The parameters of the gas in the critical section are determined from the following expressions:

$$w_c = \sqrt{2g \frac{k}{k+1} p_i v_i} = \sqrt{2g \frac{k}{k+1} RT_i} \qquad (2)$$

$$p_c = p_i \left(\frac{2}{k+1}\right)^{\frac{k}{k-1}} \tag{3}$$

$$T_c = T_i \left(\frac{p_c}{p_i}\right)^{\frac{k-1}{k}} \tag{4}$$

$$v_c = v_i \left(\frac{p_i}{p_c}\right)^{\frac{1}{k}} \tag{5}$$

Beyond the critical section the third part of the nozzle begins in the form of a diverging cone. The cone angle α is generally chosen from 8° to 12°. The fourth part of the nozzle is computed graphically. In order to make use of the method of characteristics in constructing the boundaries of the flow, it is necessary to know the value of the velocity in the direction of the lines of flow at the start of the fourth part and the area in this section and the direction of the wall of the third part must be known. Knowing the cone angle the position of the wall of the third part is determined and therefore also the direction of the streamlines at the beginning of the fourth part of the nozzle.

Taking any section x at a certain distance from the critical section and being given the ratio of the velocity w_x in the section x to the velocity in the critical section w_c, that is, w_x/w_c, the area of the nozzle at section x is found, that is, at the beginning of the fourth part from the following relations:

$$f_x = f_c \frac{w_c}{w_x} \frac{v_x}{v_c} \tag{6}$$

or

$$f_x = \frac{G v_x}{w_x} \tag{7}$$

The entire graphical computation of the nozzle is conducted with the aid of two graphs; (1) the vector diagram of

the velocities in the system of coordinates v_r, v_z, the radial velocities being laid off on the v_r axis and the axial velocities on the v_z axis, and (2) the graph of the axial section of the nozzle (half of it) in the system of coordinates r, z, the axis z coinciding with the axis of symmetry of the nozzle and r being the variable radius of the inner surface of the nozzle. The direction of the Mach lines is laid off from this curve.

The direction of the Mach lines is determined from the Prandtl—Busemann method with the aid of a rotating semi-ellipse made of a transparent material (celluloid or tracing paper). The semiaxes of the ellipse (fig. 30) are $a = 1$ and $b = \sqrt{\frac{k+1}{k-1}}$ where k is the specific heat ratio (for diatomic gases $k = c_p/c_v = 1.405$). For the value $a = 1$ any linear magnitude (100, 200 mm, etc.) may be assumed with the condition, however, that the scale of the ellipse and velocity diagrams should be the same. The scale of the geometric parameters of the nozzle is not connected with the scales of the ellipse and velocity diagrams. In general the entire construction, both the vector diagram and the axial cross-section of the nozzle may be made in absolute units.

In constructing the wall of the fourth part of the nozzle the condition is assumed that the streamlines at the initial section of this part (section x) are straight and radially directed from the point of intersection of the nozzle axis with the direction of the walls of the third part. The potential line in this case will be an arc of a circle with its center at the point of intersection of the streamlines. The radius of this arc in the coordinates $v_r v_z$ will, therefore, be equal to the chosen ratio w_x/w_c (assumed scale) and in the coordinates r, z its value is determined by the diameter of the critical section and the divergence angle of the nozzle.

After determination of the magnitude and direction of the velocity in the intial section of the fourth part of the nozzle, proceed to the graphical construction of the walls of this part.

For greater clearness the illustrative computation with numerical data is made. The nozzle is designed to give a flow with the following parameters:

$p_a = 1.033$ kg/cm^2 static pressure in the flow

$T_a = 288°$ abs. temperature of the air in the flow

$v_a = 0.815$ m^3/kg specific volume of the air in flow

$w = 900$ m/sec velocity of the flow

$G = 1.5$ kg/sec rate of discharge of air through the nozzle

Then

$$f_a = \frac{Gv_a}{w} = \frac{1.5 \times 0.815}{900} = 1.36 \times 10^{-3} \text{ m}^2$$

whence

$$d_a = 41.6 \text{ mm} \cong 42 \text{ mm}.$$

The thermodynamic parameters of the air in the chamber (before expansion in the nozzle) is determined

$$T_i = \frac{T_a}{\epsilon^{\frac{k-1}{k}}} = 691° \text{ abs.}$$

$$v_i = v_a \epsilon^{\frac{1}{k}} = 0.09125 \text{ m}^3/\text{kg}$$

$$p_i = \left[\left(\frac{w_a}{760}\right)^2 + 1\right]^{3.5} = 21.5 \text{ atm.}$$

where

$$\epsilon = \frac{p_a}{p_i} \text{ and } k = 1.401$$

Since w_i is small by comparison with w_c and w_a it is neglected in what follows.

Knowing the initial conditions the geometric and thermodynamic parameters in the critical section with the aid of formulas (1) to (5) may be determined. Carrying out the corresponding computations

$$f_c = 0.000464 \text{ m}^2$$

hence

$$d_c = \sqrt{\frac{f_c}{0.785}} = 24 \text{ mm};$$

$$w_c = 481 \text{ m/sec}$$

$$p_c = 11.35 \text{ kg/cm}^2$$

$$v_c = 0.144 \text{ m}^3/\text{kg}$$

To determine the parameters at the start of the fourth part, that is, at section x there is assumed

$$\frac{w_x}{w_c} = 1.05, \text{ i.e.} \qquad w_x = 1.05 \quad w_c = 505 \text{ m/sec}$$

Then

$$p_x = p_i \left[1 - \frac{w_x^2}{2g \frac{k}{k-1} RT_i}\right]^{\frac{k}{k-1}} = 10.6 \text{ kg/cm}^2$$

$$v_x = v_i \left(\frac{p_i}{p_g}\right)^{\frac{1}{k}} = 0.1505 \text{ m}^3/\text{kg}$$

The area at section x will be

$$f_x = \frac{Gv_x}{w_x} = 456 \text{ mm}^2$$

whence

$$d_x = 24.2 \text{ mm}$$

1. Proceeding to the graphical construction of the wall of the fourth part of the nozzle prepare a semiellipse of the type shown on figure 30 on a special sheet of tracing

paper. It is assumed that $a = 1 = 100$ millimeters and the semiaxis $b = \sqrt{\frac{k+1}{k-1}} = \sqrt{\frac{1.4+1}{1.4-1}} = 2.45$ units, that is, $b = 245$ millimeters.

2. On a separate sheet of paper draw the coordinate axes v_r, v_z (the vector diagram of the velocities, fig. 31). From point 0 draw a straight line at the angle $\alpha/2 = 6^\circ$. With radius $r = 1.05 = 105$ millimeters and center 0 an arc intersecting the v_z axis is described. The segment of the arc included in the sector with angle $\alpha/2$ gives the velocity distribution at the initial section of the fourth part. On this arc points 1, 2, and 3 are arbitrarily denoted. The lines 0-1, 0-2, and 0-3 are the velocity vectors for this section.

Simultaneously with the construction of the vector velocity diagram construct the upper half of the axial section of the nozzle (fig. 32) bearing in mind that the points on the graph of figure 32 and the end of the corresponding vectors in figure 31 are denoted by the same figure.

3. Determine the Mach lines passing through the points 1, 2, and 3 (fig. 32). For this purpose the semiellipse (on tracing paper) is placed with its center (point 0) on point 0 on figure 31 (fastened with a pin). On rotating the semiellipse about its center find the position for which the curve of the ellipse falls on point 1 (there may be two such postions), the direction of the Mach line is drawn parallel to the major semiaxis (b) through point 1, figure 32. In the same manner determine the direction of the Mach lines through points 2 and 3. At these points the Mach lines are drawn for two directions according to the two possible positions of the major axis of the semiellipse. Point 4 (fig. 32) is obtained as the point of intersection of the Mach lines through points 2 and 3 and point 5 as the point of intersection of the Mach lines through points 1 and 2.

4. The velocities at the points 4 and 5 are determined in the following manner: through point 2 (fig. 31) draw a straight line parallel to the second Mach line passing through the point 3 (but not 3 to 4). On the line drawn through point 2 (fig. 31) take a segment equal to $\delta = a^2 v_r ds/w^2 r$, where w is the velocity at point 2 (equal

to the vector $\overline{02}$), $a = \sqrt{\frac{k+1}{2}\frac{k-1}{2}w^2}$ the velocity of sound at this point, v_r the component of the velocity along the normal to the axis, r the distance of point 2 (fig. 32) from the axis, and ds the magnitude of the segment $\overline{2-4}$ (fig. 32). For point 3 the segment δ is determined in the same way. In computing a the value of w is determined from the vector diagram in linear units and to the same scale to which the diagrams are drawn. The magnitudes r and ds are determined on the diagram in millimeters; v_z is measured from the graph of figure 31 with account taken of the scale.

The question as to the direction in which the segment δ should be laid off is solved by the following rule of signs. The segment δ is laid off to the right, that is, the projection of the vector δ on the v_z axis has a positive direction in case the product $v_z\, d_z\, (v_z^2 - a^2)$ is positive; otherwise the segment δ is laid off to the left.

The magnitude d_z is the axial component of the velocity (fig. 32). For example, for point 2 (fig. 32) d_z is equal to the segment $\overline{2-4}$ (in the general case d_z is equal to the vector from the point at which the velocity is known to the point where it is sought). For the point 2 the magnitude v_z is positive, the values $v_r^2 - a^2$ and d_z are also positive and therefore the segment is positive. The same is true for point 3.

At the ends the segments δ are drawn perpendicular with intersection point 4 (fig. 31). Connecting point 4 with the origin of coordinates the vector $\overline{0-4}$ which determines the velocity at point 4 (fig. 31) is obtained. To determine the velocity vector $\overline{0-5}$ (fig. 31) it is is necessary to determine the value of the segment δ at point 1. For the center of the jet $r = 0$ and $v_r = 0$. Hence to determine point 5 the values of v_r and r are assumed the same as for the neighboring point 2.

5. Determine, by the method already described, the Mach lines through the points 4 and 5 (fig. 32). The point 6 (fig. 32) is determined as the point of intersection of the Mach line through point 5 with the z axis and point 7 as the point of intersection of the Mach lines through points 4 and 5.

6. Determine the velocities at points 6 and 7. Through point 4 (fig. 31) draw a straight line parallel to 47 (fig. 32) and parallel to the Mach line through point 4 (fig. 32). Draw through point 5 (fig. 31) parallels $\overline{57}$ and $\overline{56}$ (fig. 32). On the straight lines lay off the segments δ. From the ends of the segments δ draw straight lines normal to them, the intersection of which gives points 6 and 7. The vectors $\overline{06}$ and $\overline{07}$ are the vector velocities at points 6 and 7 (fig. 32).

7. Determine the Mach lines through points 6 and 7 (fig. 32). Point 8 is determined as the point of intersection of the Mach lines through points 6 and 7.

8. Determine the velocity at point 8 (fig. 32). For this purpose draw through point 7 (fig. 31) a straight line parallel to the Mach line through point 7 (but not $\overline{78}$); through point 6 (fig. 31) a parallel to the Mach line through point 6 (but not $\overline{68}$). On the straight lines lay off the segments δ. It should be noted that at point 6 the value $v_r = 0 = r$ hence the value of δ for point 6 is taken corresponding to point 7. From the ends of δ draw straight lines perpendicular to δ. Their intersection will give point 8 (fig. 31).

9. Determine the Mach lines through point 8 (fig. 32). Point 9 is determined as the point of intersection of the Mach line through point 8 with the axis.

10. Determine the velocity at point 9. For this purpose through point 8 (fig. 31) draw a straight line parallel to the line through point 8 (fig. 32) (not $\overline{89}$). On this straight line lay off the segment δ. From the ends of the segment δ and perpendicular to the latter draw a straight line whose intersection with the v_z axis will give point 9.

Having determined point 9 the character of the flow in the entire triangle of definition 1, 3, and 9 is obtained, that is, that part of the flow which is entirely determined by the distribution of the velocity in the initial section and on which the part of the wall lying to the right of the initial section has no effect.

Next solve the problem of what shape it is necessary to give the nozzle wall for a given velocity distribution at the initial section in order to obtain, at the outlet section, a velocity constant in magnitude and direction. This velocity should be equal to the velocity at the point

9 and, therefore, the Mach line from point 9 will be straight.

11. Draw the Mach line through point 9 (fig. 32). On it take a number of points denoted by 9 with a subscript. The velocities at these points will all agree with the vector $\overline{09}$ (fig. 31).

12. Determine the point 10 which is the point of intersection of the Mach line through 8 and the second point 9.

13. Determine the velocity at point 10. To do this, draw through point 8 (fig. 31) a straight line parallel to $\overline{89}$ (fig. 32) and on it lay off the segment 8. From the end of the latter draw a perpendicular line to intersect with the straight line from point 9. The point of intersection will be the end of the velocity vector at point 10.

14. Determine the point 11 (fig. 32), which is the point of intersection of the Mach lines through points 7 and 10.

15. Determine the velocity at point 11. The vector $\overline{0 - 11}$ is the velocity vector at point 11.

16. Determine point 12 (fig. 32), which is the point of intersection of the Mach lines through points 4 and 11. Determine the velocity at point 12. For this purpose draw through point 4 (fig. 31) a straight line parallel to the segment $\overline{47}$ (fig. 32) and through point 11 a line parallel to the segment $\overline{7 - 11}$. The vector $\overline{0 - 12}$ determines the velocity at point 12.

17. Determine point 13 (fig. 32), the point of intersection of the Mach lines through points 10 and 9.

18. Determine the velocity at point 13 (fig. 32). The vector $\overline{0 - 13}$ is the velocity vector at point 13 (points 13 and 10 (fig. 31) practically coincided).

19. Determine point 14 (fig. 32), which is the point of intersection of the Mach lines through points 11 and 13.

20. Determine the velocity at point 14. For this purpose through point 11 (fig. 31) draw a line parallel to

$\overline{10-11}$ (fig. 32) and through point 13 (fig. 31) draw a line parallel to $\overline{10-13}$ (fig. 32).

21. Determine the point 15 (fig. 32) which is the point of intersection of the Mach lines through 13 and 9.

Thus a sufficient number of points in the angular space 399 have been determined.

22. The generator of the wall is obtained in the following manner: through point 3 (fig. 32) draw a straight line in the radial direction, that is, prolong the wall of the third part to intersect with the segment $\overline{4-12}$ and the point of intersection a is obtained.

The velocity at point a is obtained by linear interpolation, that is, the segment $\overline{4-12}$ (fig. 31) is divided in the same ratio in which a divides the segment $\overline{4-12}$ (fig. 32). The vector $\overline{oa}$ (fig. 31) thus obtained gives the direction of the following segment of the wall generator to the intersection with $\overline{11-12}$ which is drawn in figure 32 parallel to the segment $\overline{oa}$, and so forth, prolonged to intersect with the line 99 and the latter point of intersection gives us the outlet section. For greater clarity the point a and similar points are not shown on the diagram.

The results of the computation by the graphical construction are collected in a table. The velocity w, obtained at the outlet section, may be less than or greater than the velocity which must be obtained since the ratio w_x/w_c was arbitrarily assumed. Assuming, successively, the values $w_x/w_c = 0.2$, 1.5, 1.8, and so forth, w/w_c is obtained for each ratio w_x/w_c. From the obtained values of w/w_c for different w_x/w_c draw the curve of w/w_c as a function of w_x/w_c (fig. 33). From the curve find the values of w_x/w_c required for the given velocity. As may be seen from the curve, for $w/w_c = 900/481 = 1.87$ the value of $w_x/w_c = 1.67$. It should be noted that the curve on figure 33 is true only for the divergence angle $\alpha = 12^0$ and for the discharge rate $G = 1.5$ kg/sec assumed in the computation. The vector velocity diagram and the nozzle section obtained for the given velocity with $w_x/w_c = 1.67$ are shown in figure 34. The equivalent Laval nozzle (the straight line generating the wall) is shown dotted.

Translation by S. Reiss,
National Advisory Committee
for Aeronautics.

REFERENCES

1. Iurév, B. N.: Experimental Aerodynamics. Pt. I, p. 84.

2. Idelchik, I. E.: Investigation of the Nozzle of Wind Tunnels. Rep. No. 80, CAHI, 1935.

3. Witoszynski, C.: Ueber Strahlerweiterung und Strahlablablenkung. Vorträge aus dem Gebiete der Hydro—und Aerodynamik, 1922.

4. Frankl, F. I.: Supersonic Flows with Axial Symmetry. Investia Art, Akademii RKKA, Vol. I, 1934.

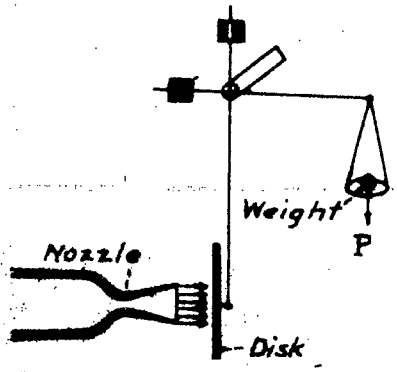

Figure 1.- Apparatus for measuring the impulse of a jet with dynamometer and disk.

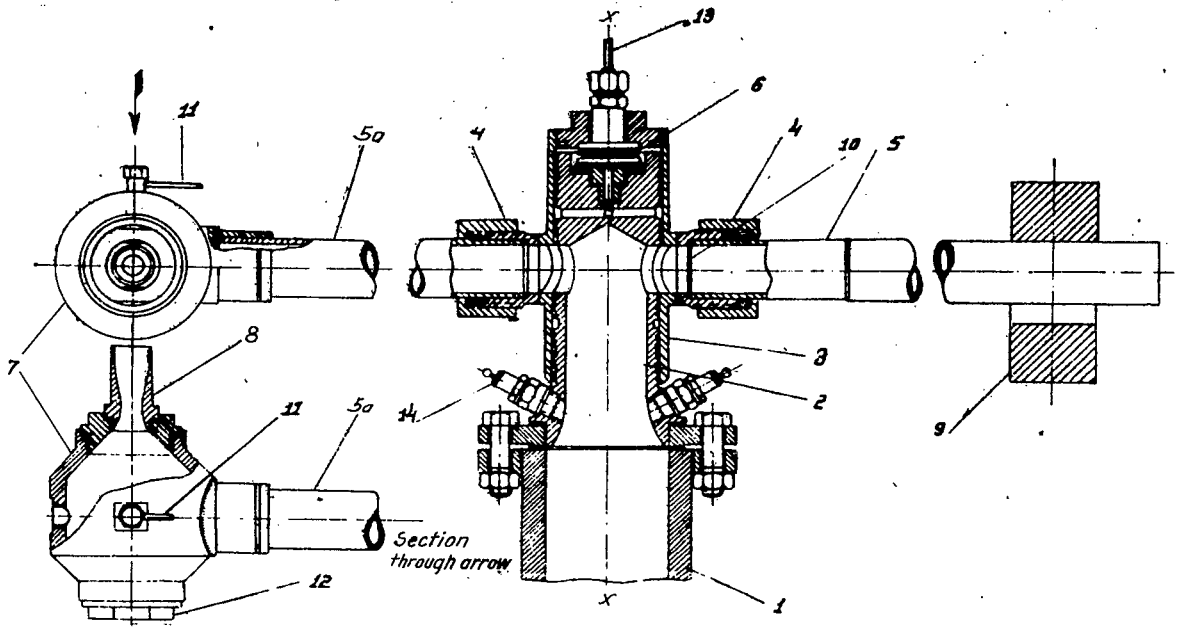

Figure 2.- Sketch of apparatus for measuring the reaction force of a jet.

Figure 3.- General view of the apparatus sketched in Fig. 2.

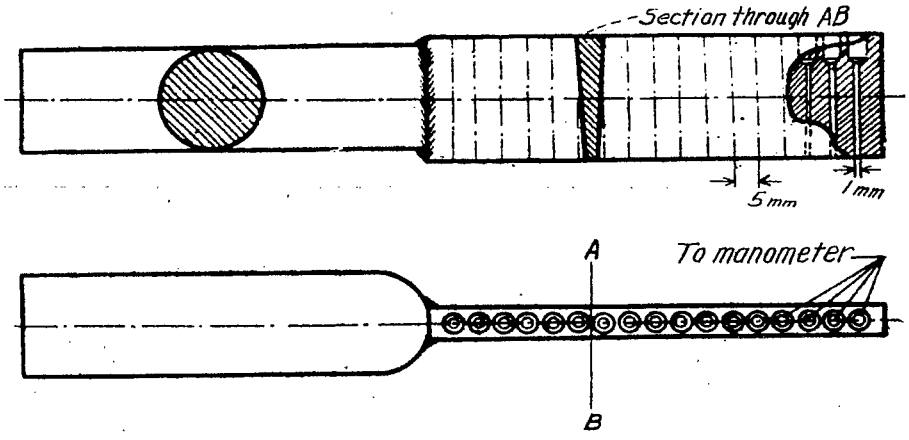

Figure 4.- A battery of Pitot tubes.

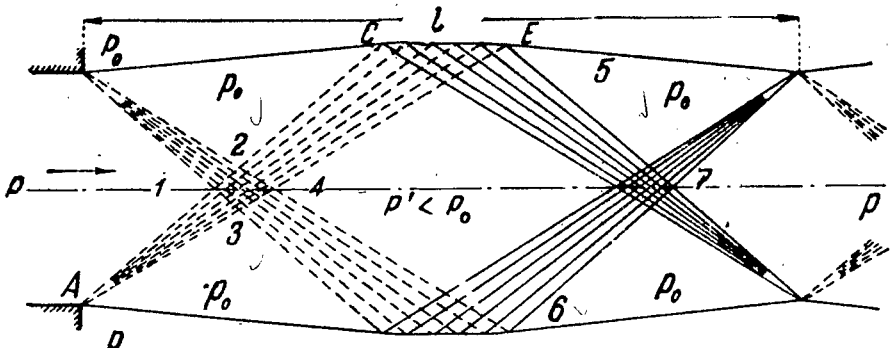

Figure 10.- Scheme of two-dimensional supersonic flow for $p_a > p_0$.

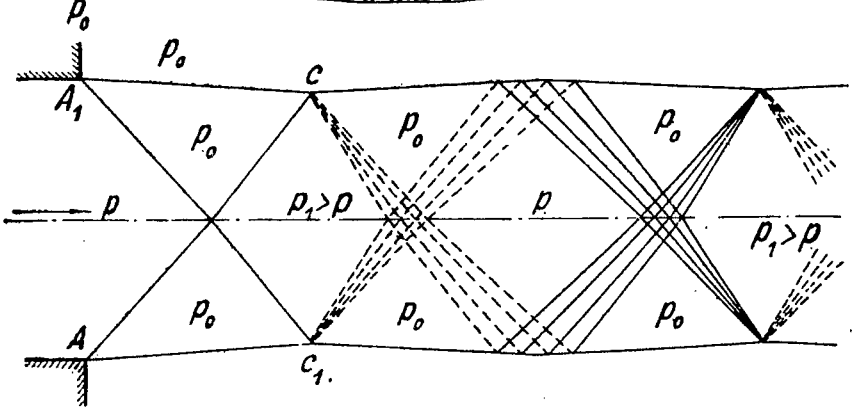

Figure 11.- Scheme of two-dimensional supersonic flow for $p_a < p_0$.

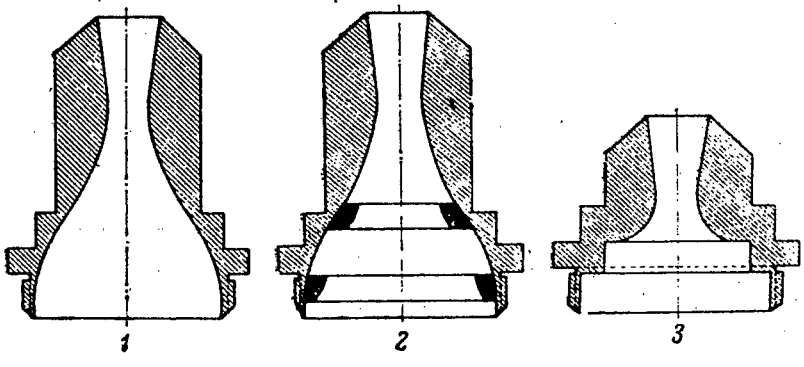

Figure 16.- Sketches of nozzles for studying the effect of the inlet part.

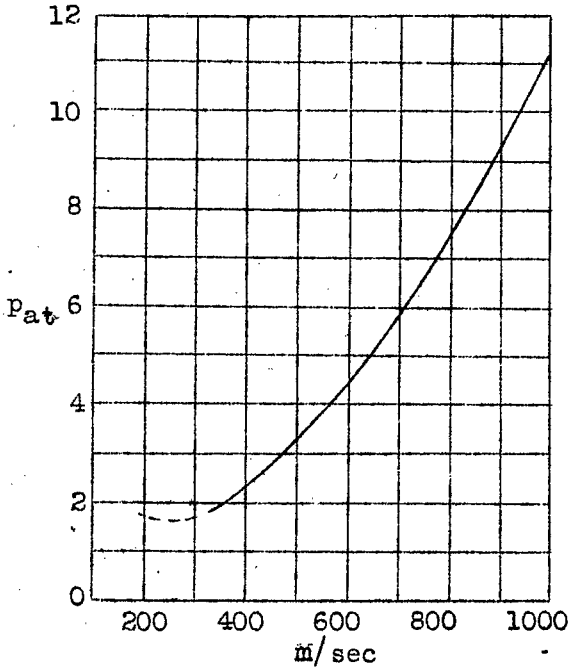

Figure 5.- Dynamic pressure in supersonic flow computed by the Raleigh formula.

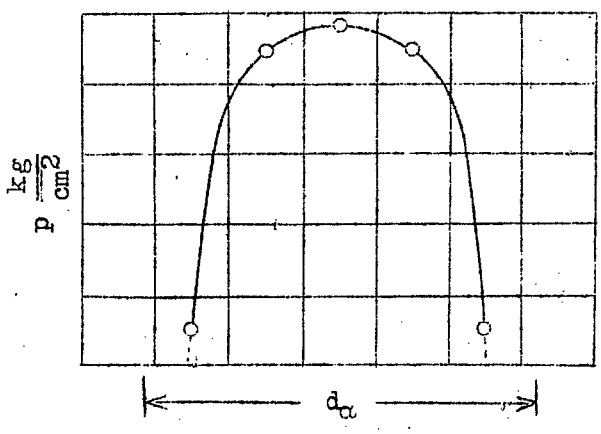

Figure 7.- Velocity distribution in the transverse cross-section of a jet from a conical Laval nozzle.

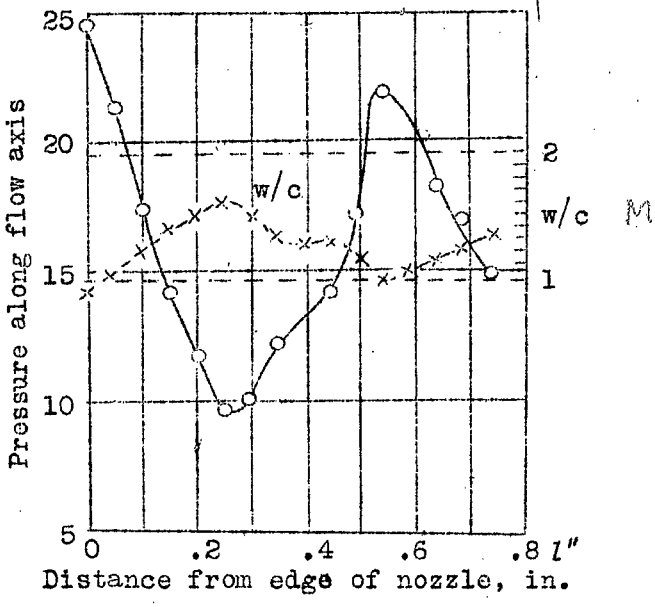

Figure 8.- Velocity and static pressure distribution along the axis of a jet from a Laval nozzle.

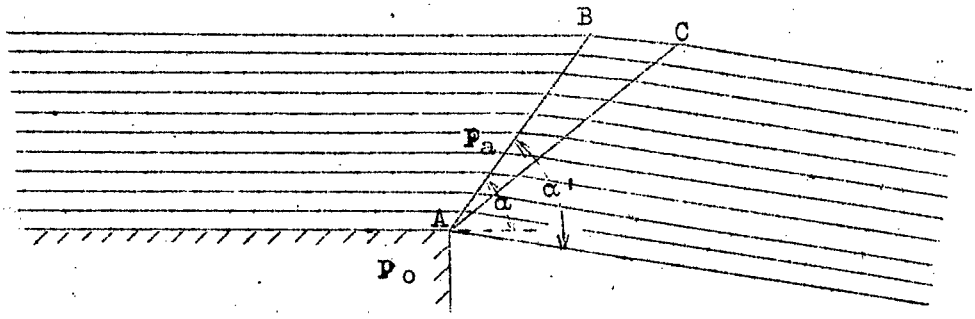

Figure 9.- Two dimensional supersonic flow.

Figure 6.- Mounting of static tube in flow.

Figure 12.- Spectrum of flow showing sucked in air.

Figure 24.- Flow spectrum for the conical nozzle.

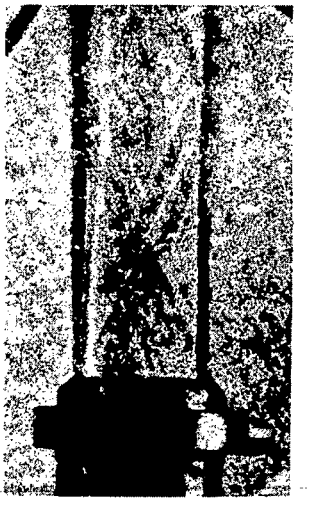

Figure 25.- Flow spectrum for the Frankl nozzle.

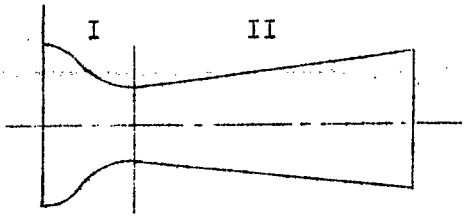

Figure 13.- Sketch of conical nozzle.

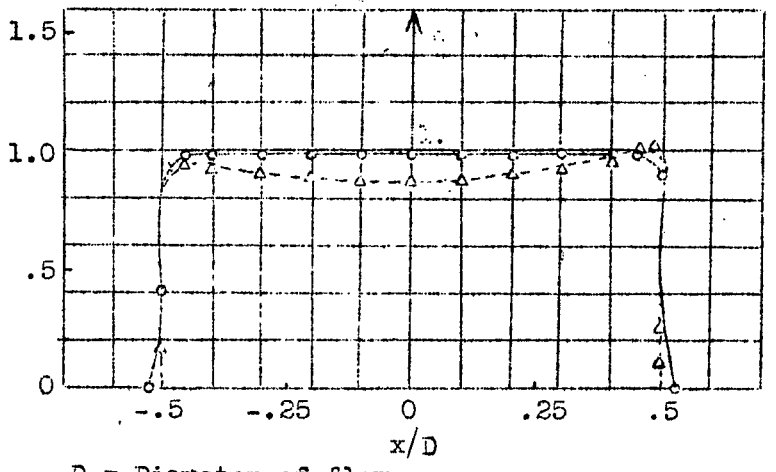

Figure 14.- Distribution of dynamic pressure for two nozzles with different shapes of inlet parts (x = 20 mm).

D = Diameter of flow.
x = Distance from outlet section.

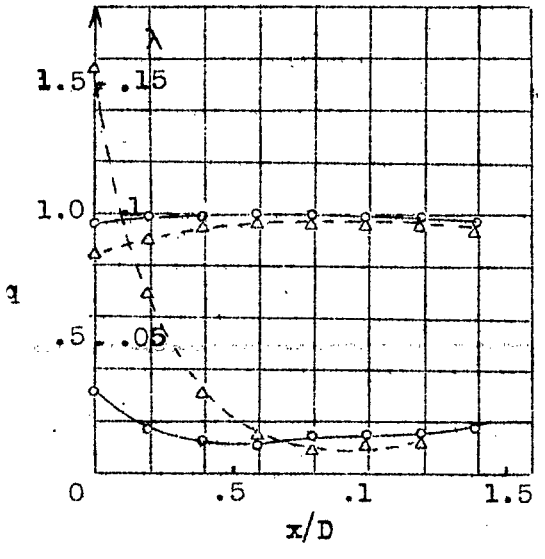

Figure 15.- Dynamic pressure and velocity distributions for two nozzles with different shapes of inlet parts (along the flow axis in the working part).

D = Diameter of flow.
x = Distance from nozzle outlet.

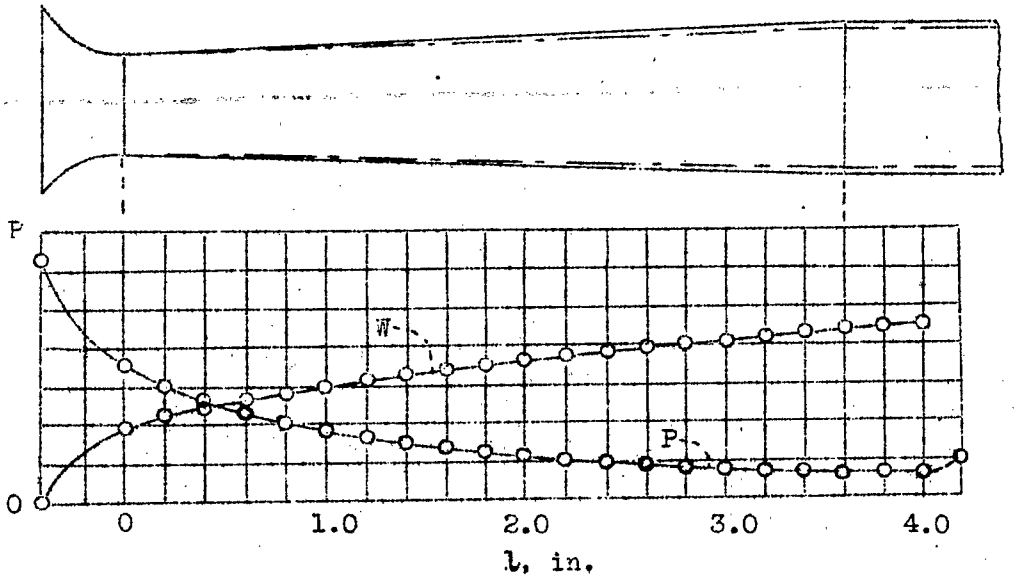

Figure 17.- Curves of variation of the static pressure and velocity for the Stanton nozzle.

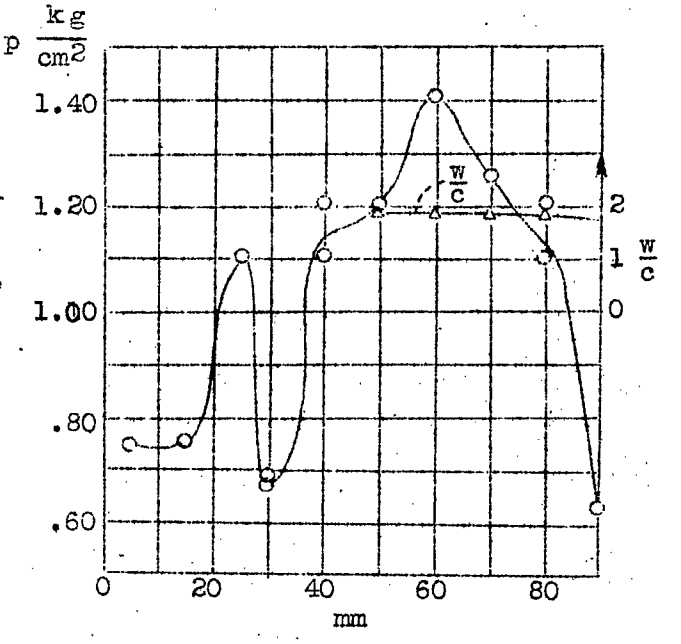

Figure 18.- Static pressure and velocity distributions along the flow axis for the conoidal nozzle. The nozzle was computed for w = 1.82c.

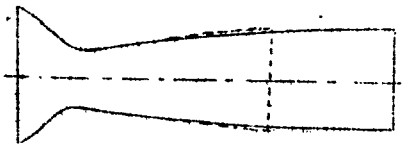

Figure 20.- Contour of nozzle constructed by the method of Prof. Frankl.

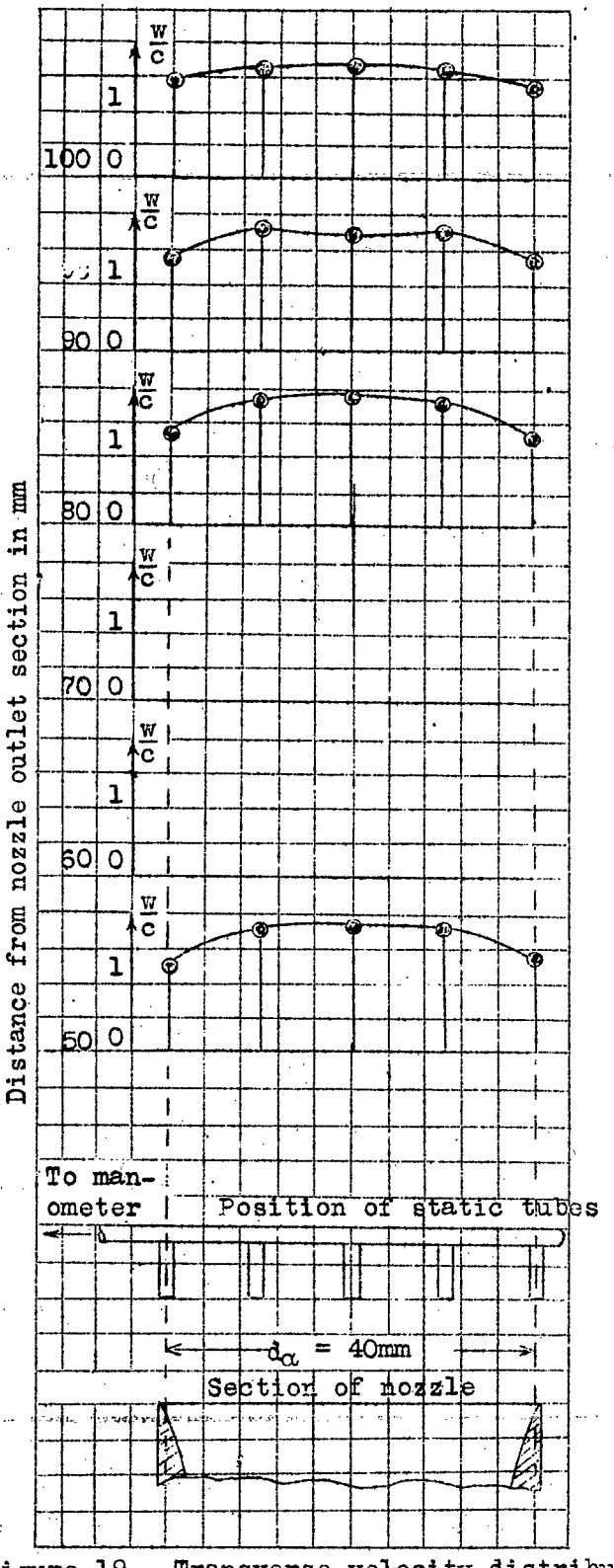

Figure 19.- Transverse velocity distribution for the conoidal nozzle.

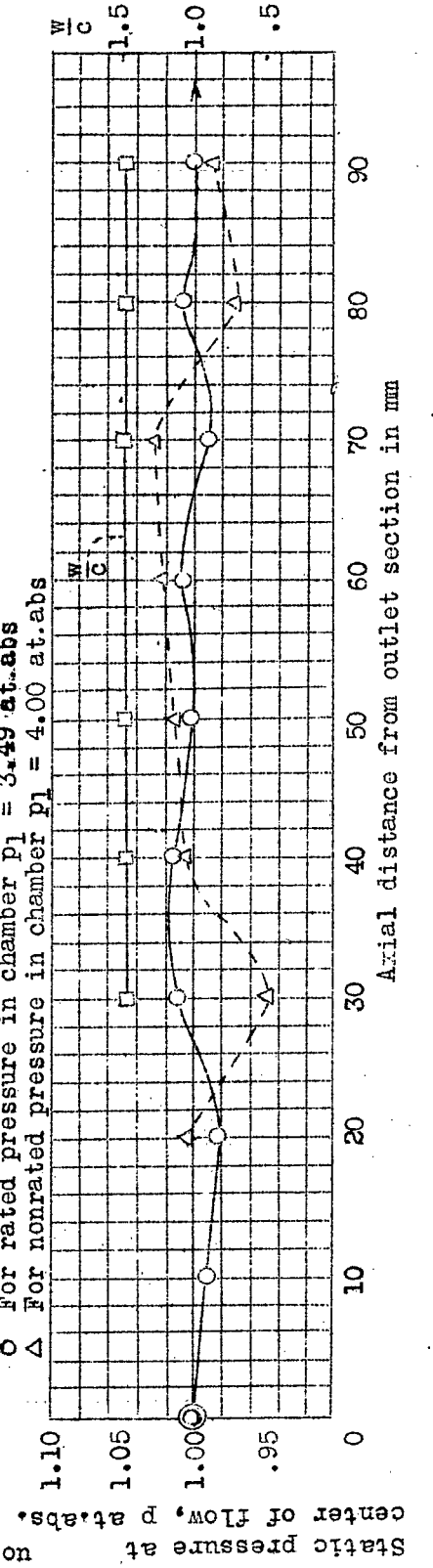

Figure 21.- Axial static pressure and velocity distributions for w/c = 1.47.

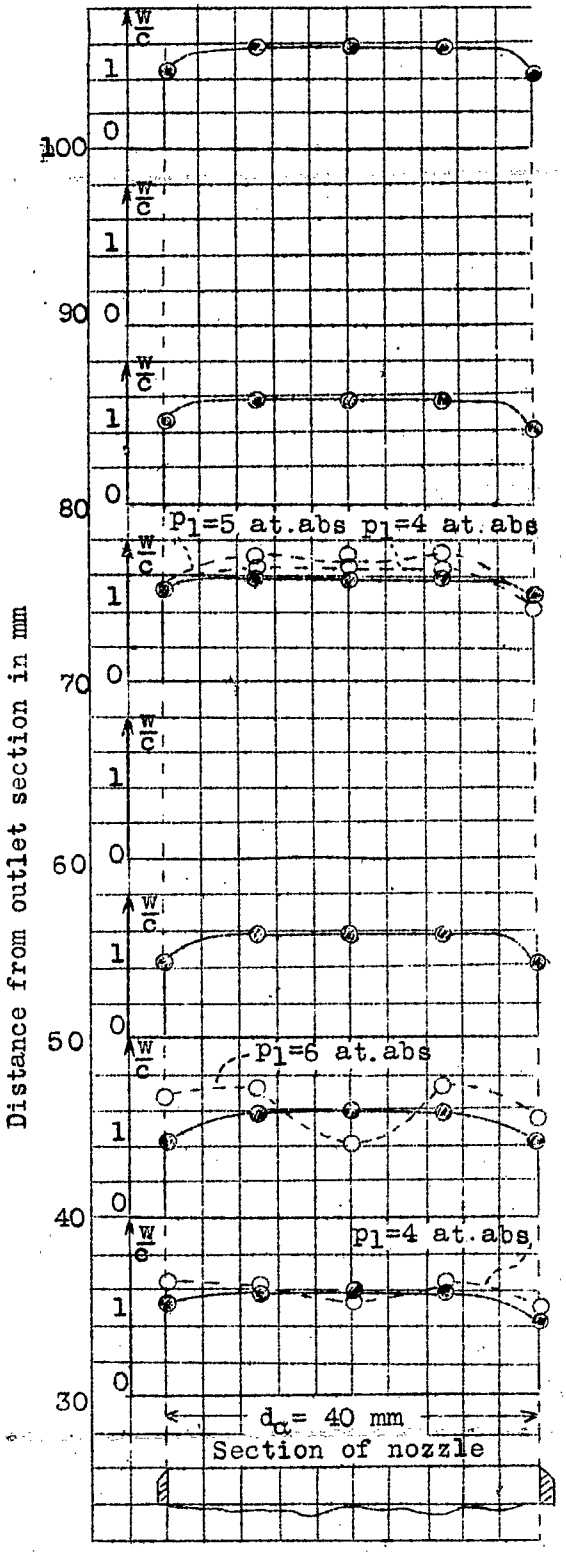

Figure 22.- Transverse velocity distribution for w/c = 1.47.

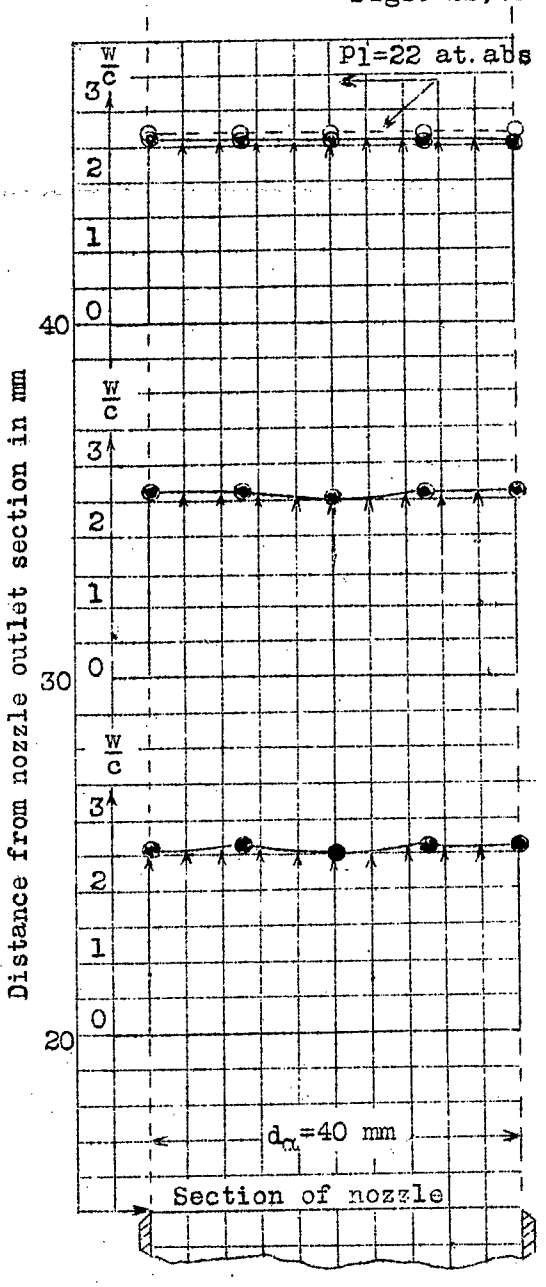

Figure 23.- Transverse velocity distribution for w/c = 2.64.

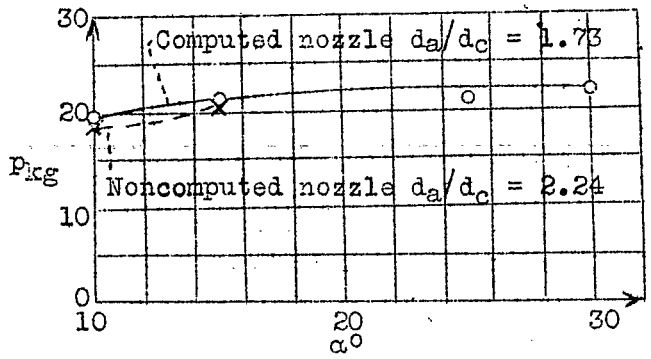

Figure 26.- Dependence of the reaction of the jet on the divergence angle of the nozzle.

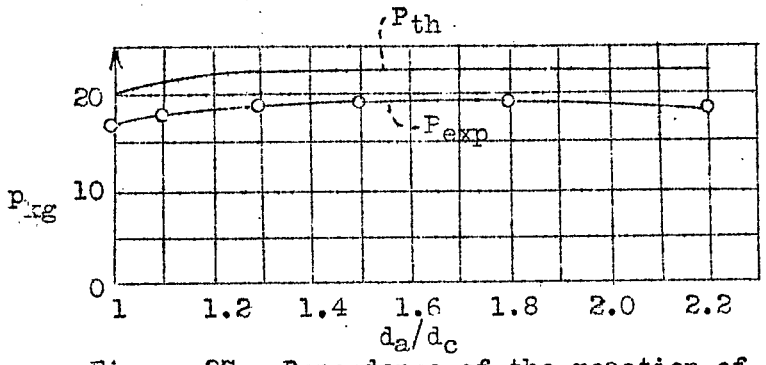

Figure 27.- Dependence of the reaction of the jet on d_a/d_c.

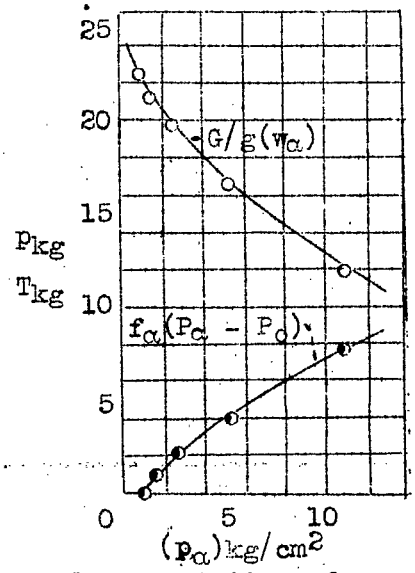

Figure 28.- Variation of mw and Δp with p_α.

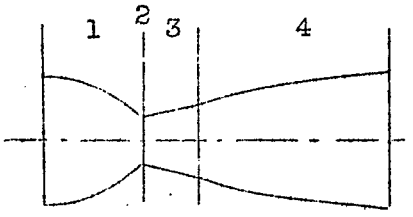

Figure 29.- Nozzle contour.

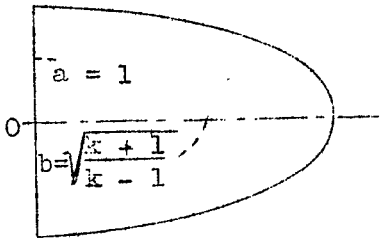

Figure 30.- Ellipse.

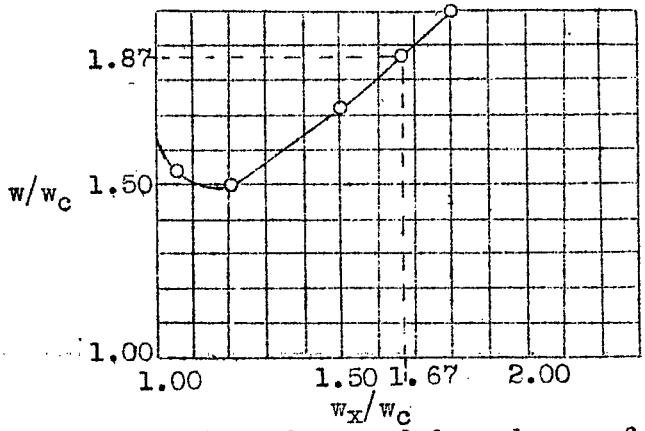

Figure 33.- Curve of dependence of w/w_c on w_x/w_c.

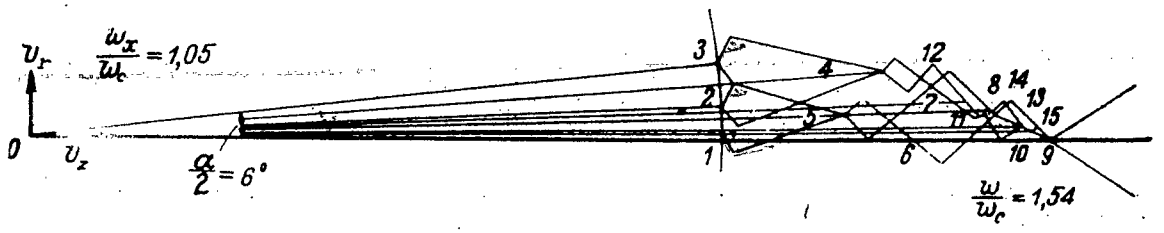

Figure 31.- Velocity vector diagram.

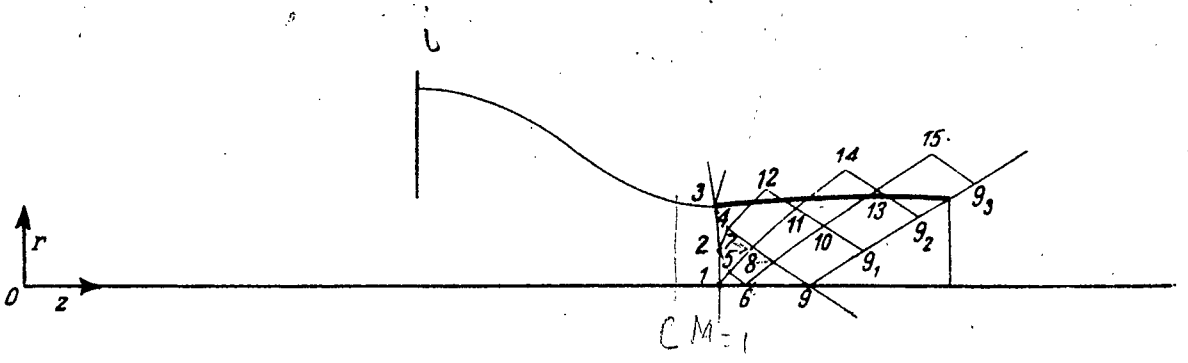

Figure 32.- Axial section of the nozzle.

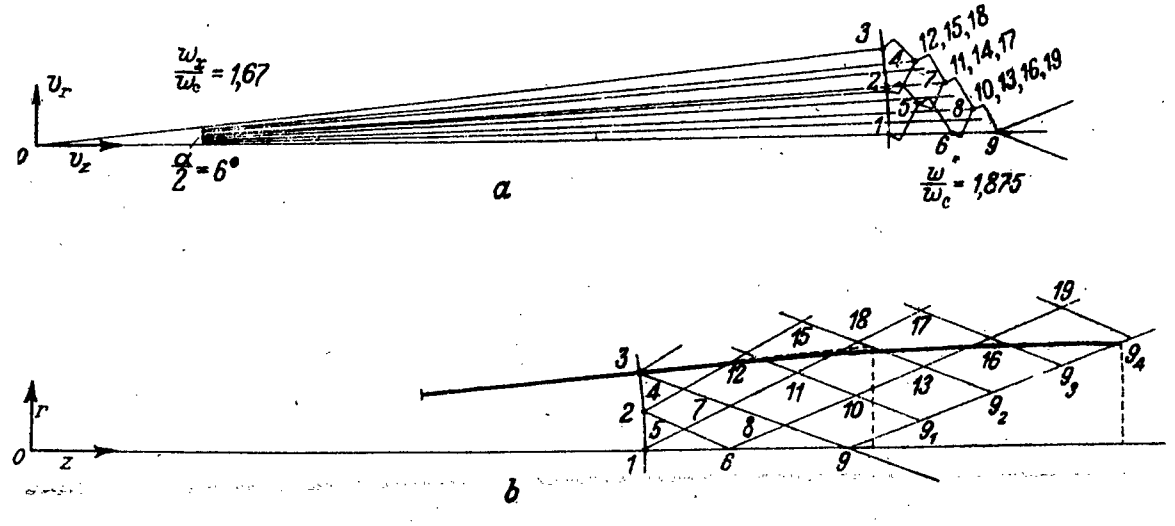

Figure 34.- Vector velocity diagram and axial section of the nozzle for w = 900 m/sec.